Validating and comparing frequency-domain electromagnetic database inversion for top layer estimation

H. Tatar

Applied Geophysics

TUDelft
Delft University of Technology

Faculty of Civil Engineering and Geosciences

Validating and comparing frequency-domain electromagnetic database inversion for top layer estimation

MASTER OF SCIENCE THESIS

For the degree of Master of Science in Applied Geophysics at Delft University of Technology

H. Tatar

Applied Geophysics

August 8, 2020

IDEA League

FUGRO

TU Delft
Delft
University of
Technology

Abstract

Clay has been used for many hundreds of years in building dikes. Their physical properties and thickness are essential for a dike to maintain its function. For the last fifteen years electromagnetic induction instruments (EMI) have been playing a growing role in mapping electromagnetic soil properties. Layered models with sharp boundaries between different soil units represents the soil profile accurately. Therefore, two database inversion procedures are developed and proposed. Synthetic data sets and field measurements have been used to validate and compare our retrieved electrical conductivity/resistivity models. Field measurements of a so-called multi-receiver EMI instruement (CMD-Explorer and CMD-MiniExplorer) have been used to perform the database inversion on, and are being compared to ERT data and hand drill data. The EMI instruments (CMD-Explorer and CMD-MiniExplorer) consisting of three receiving antennas, fixed operating frequency and two measurement configurations will not allow us more information than of a estimate three-layered model.

Therefore, the calibration process here proposed is based on finding the best fit of the electromagnetic responses (in the least squares sense) in a 5-D solution space created by calculating the electromagnetic responses using five medium parameters and the layered earth response. These medium parameters are the three layered conductivity's and thicknesses of the first two layers. Using these five medium parameters, a database is built based on predefined ranges of medium parameters and is being used to perform the inversion procedure with.

Two methods of inversion have been proposed: constrained and full database inversion. The synthetic models have been recovered with an average data misfit of 0.0096 and 0.0032 for the constrained data base inversion for respectively model 1 and model 2. For the full database inversion data misfit values of 0.00316 and 0.0021 were accomplished. Comparing ERT and electrical resistivity obtained from EMI measurements, one could see that the trend and first two layer thicknesses were recovered. Verifying EMI measurements using hand drill data, we were able to recover the top layer at few locations.

Contents

Acknowledgements

"The important thing is not to stop questioning. Curiosity has its own reason for existing."
— *Albert Einstein*

Chapter 1

Introduction

1-1 The function of clay in dike bodies

Clay is being used for dikes for many hundreds of years, exclusively for top layers and the core of the dike. The soil type is known for its good erosion resistance and shape retention. These properties are useful for steep banks and especially if water already laps against the bank. The physical properties of clay are crucial for the selection of clay for dike constructions.

Nowadays, clay is still being used for dike constructions, a clay-containing top layer with the purpose of giving soil-mechanical stability to the entire dike body. Figure 1-1 shows constructive parts of a dike body in which clay is used.
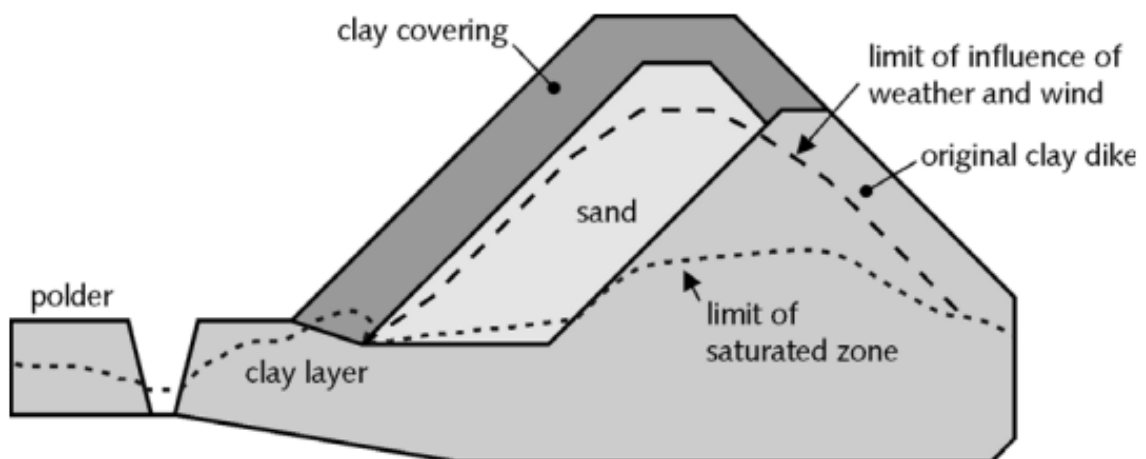
Figure 1-1: Dike profile
[6]

In general intact clay is seen as a body without structure, however when groundwater fluctuates and it gets in contact with clay, it will have an impact on the clay and the structure. The latter can also happen due to animal or plant activity. This results in a increase of hydraulic permeability because fracture networks may develop.(See Figure 1-2)

Clay containing a structure consists of a composition of larger and smaller mainly angular lumps, the so-called 'soil aggregate'. The larger soil aggregates generally fall apart into smaller aggregates,with dimensions of less than 2 mm, which can be found directly under the grass sod.

A structure present in the core of a dike can have significant negative influence on the function of clay cores in dikes.

Figure 1-2: Soil structure of clay in dikes with the influence of burrowing animals and root penetration. The structure underneath is the result of change in moisture content.
[6]

1-2   Soil mechanics

1-2-1   Soil mineralogy

Silts, sands and gravel are classified by their size and may consist of a variety of minerals. Due to the stability of quartz compared to other rock minerals, quartz is the most common component of sand and silt. Other common minerals present in sand and silts are mica and feldspar[19]. The mineral composition of gravel may be comparable to the minerals of the parent rock.

The common clay minerals are smectite, illite and kaolinite. These minerals often form in sheet or plate-like structures, with lengths ranging between 10^{-7}m and 4×10^{-6} m and thicknesses ranging between 10^{-9} m and 2×10^{-6} m. Clay minerals have a relatively large specific surface area in the range of 10 to 1000 square meters per gram of solid[23]. The specific surface area is defined as the ratio of the surface area of particles to the mass of the particles. Due to the large surface area available for chemical, electrostatic, and van der Waals interaction, the mechanical behavior of clay minerals is very sensitive to the amount of pore fluid available and the type and amount of dissolved ions in the pore fluid[19].
To predict the effect of clay on the way a soil behaves, it is necessary to know the types of clay and the amounts present. Soils containing a certain high-activity of clay minerals make very unstable material, which will swell when it is wet and shrink when dry. This shrink-and-swell phenomenon can easily cause retaining walls to collapse. These clays become quite sticky and challenging to work with. Meanwhile, low-activity clays, which are formed under different conditions, can be very stable and easy to process.

Soil minerals are generally formed by atoms of oxygen, silicon, hydrogen and aluminium, organized in various crystalline forms. These elements along with calcium, sodium, potassium, magnesium, and carbon constitute over 99 per cent of the solid mass of soils[19].

1-2-2   Grain size distribution

Soils consist of a mixture of particles of different size, shape and mineralogy. Since the size of particles has an important effect on the soil behaviour, the grain size and it's distribution are used to classify soils. The grain size distribution describes the relative proportions of particles of different sizes. Generally, the grain size distribution is visualized in a cumulative distribution graph. This graph consists of percentages of particles finer than a grain size as a function of the size. The median grain size,

The soil particle types are classified by performing tests on disturbed samples of the soil. This provides information about the properties of the grains. Classification of the types of grains present in a soil does not take into account any important effect of the structure or fabric of the soil. The terms structure and fabric describe the compactness of the particles and patterns in the arrangement of particles in a support structure, as well as the pore size and pore fluid distributions. In contrast to geotechnical engineers, engineering geologists also classify the soils according to their origin and depositional history.

The Unified Soil Classification System (USCS) is often used as a soil classification system in engineering and geology. It describes the texture and grain size of a soil, and can be applied to most unconsolidated materials.

The USCS has three major classification groups: 1. coarse-grained soils (sand and gravels); 2. fine-grained soils (silts and clays); and 3. highly organic soils ("peat"). In order to interpret the three major soil groups, the USCS divide it in sub classes. Sands and gravels can be distinguished by grain size, and be classified as "well-graded"and "poorly-graded". Silts and clays are distinguished by Atterberg limits, where they are classed as "high-plasticity" or "low-plasticity" soils as well. Reasonable organic soils are considered to be subdivisions of silt and clay. They are distinguished from inorganic soils by changes in their plasticity properties (and Atterberg limits) on drying.
The Atterberg limit is a moisture content, expressed as water-to-soil mass ratio in percent[1].

1-3   Previous work

Soil electrical and magnetic properties are having a increasing role in the different aspects of near-surface geophysical surveying methods. Beside the developments in the direct current (DC) electrical methods, such as electrical resistivity tomography (ERT), the application of electromagnetic induction (EMI) instruments has become more common during the last 15 years. After the early studies for archaeological prospection [12] [28] [20] and commercializing of the low induction number (LIN) by Geonics, Ltd, the first success was achieved by allowing applications to salted soil [24]. At later stages this led to a large variety of soil studies through electrical conductivity mapping [30] [2] [25]. However, in general the use of EMI instruments remains limited when it comes to delineation of layers. Depending on the thicknesses and the difficulty that comes with calibration of these devices.

Calbiration is a problem that applies to almost all measurements, with possible exceptions for electric current source and electric potential difference measurements. Since the introduction of applied geophysics prospesctors have deployed considerable efforts to make quantitative measurements and express their results in terms of the desired quantities.

The most common and widely used method for (clay) soil layer quantification and characterization relies on shallow borehole information and ground-based geophysical survey methods. In order to be valid in regional scale and taking into account the thickness variability of a soil, a method based on field measurements needs a large database of high-density distributed field observations, which are essential in order to correctly define the co-variance model necessary to interpolate the point measurements [13] and minimize spatial aliasing. In the literature, there are examples of studies reporting collection of a large number of peat thickness measurements performed in the field using push probes [22] [11] [4]. However, even though the use of a push probe is a relatively fast method, which can result in large databases, it has been shown that the accuracy obtained using exclusively soil probes is limited. Parry et al. (2014) confirmed that it leads to an average error of depth estimation of 35 % compared to GPR depth estimations, calibrated using common midpoint (CMP) surveys [21]. Soil coring assures much higher accuracy's in measuring peat thickness locally, though this appears to be an extremely time consuming activity and so collecting large databases will be out of reach.
To overcome these issues, different common ground-based geophysical methods have been successfully applied for peat layer determination. Methods like ground penetrating radar (GPR), electrical resistivity tomography (ERT) and induced polarization (IP) methods together with borehole data can increase in more accurate peat layer determination.
In the end, the use of soil cores and these ground-based geophysical methods are limited for moist and wet soils, which are difficult to access.

Geophysical survey methods based on electromagnetic induction (EMI) have proven their potential to map soil stratigraphy over shallow depths [5]. EMI instruments measure a volume-weighted average of the soil electrical conductivity. Assuming no lateral variations, this leads to the so called depth response function [18] which expresses the relative response to the primary magnetic field created by the EMI instrument. The depth response is dependent on the instrument's coil configuration and the separation distance between transmitter and receiver.
The introduction of multi-receiver frequency-domain EM (FDEM) instruments makes it possible to obtain data over various soil volumes simultaneously. These FDEM instruments are non-destructive and can be used for a quick mapping of the lateral and vertical conductivity distribution with simplified models.

Using both hard borehole data and soft data derived from helicopter-borne frequency-domain EM measurements Gunnink et al. (2014) concluded that a 3D model of lithology was constructed that was superior to the model that was used without AEM data. The use of AEM data proved to be greatly beneficial in modelling the clay occurrence [8].

The Fugro Land Geophysics department performs FDEM measurements for different purposes. For example detecting leakages in dikes, tracing conductive objects in the subsurface, the spread of contaminated groundwater, analyzing soil structures (correlated with hand drilling) and determining sand/clay volumes.

For this measurements, Fugro use the CMD-Explorer and the CMD-MiniExplorer, which are both manufactured by GF Instruments. The CMD-Explorer (read CMD-Explorer/CMD-MiniExplorer) consists of both source and three receiver sensors, which are loop antennas, and the transmitter and three receivers, the electronics. The source and receiver sensors can be simplified in a model by magnetic dipoles. The transmitter creates the excitation pules that is passed to the transmitting antenna, which then starts to radiate an EM field. The receiving antennas induce a current because of the source antenna radiation and the earth response. The electric potential difference that is incurred across the terminals of the loop antennas connected to the receiver is measured and converted to an equivalent magnetic field and stored on disk as in-phase and quadrature (out of phase). The quadrature value is converted again to apparent conductivity using low induction numbers (LIN).

The three different source-receiver pairs have fixed separations making it possible to reach different soil volumes, including different lateral ranges as well. That is different than the user's interest, namely reaching different depth ranges. In addition, the CMD-Explorer also has two measuring configurations, these are the horizontal co-planar configuration (HCP) and the vertical co-planar configuration (VCP). Depending on the depth of interest one could decide to pick one of the configurations to measure with. The CMD-Explorer and CMD-MiniExplorer operate both at fixed frequencies, 10 kHz and 30 kHz respectively.

1-4   Thesis objective

The CMD-Explorer (and the CMD-MiniExplorer) with a fixed frequency, three receiving antennas and two measurement configurations, one cannot expect more information than estimate a three-layered model. The objective of this master thesis is to generate a database for all possible three-layered models sampled over an expected range of conductivity values of 10^{-3} S/m to $10^{-0.5}$ S/m and two layer thicknesses sampled from 0 to 5 meter.

This database needs to be validated, and calibrated by hand-drill data to make sure such a simple 1-D layered model set can adequately describe most common situations in the field.

Chapter 2

Methods

2-1 Electromagnetic fields and waves

All electromagnetic methods rely on Maxwell's equations, that describe the interaction between the electric field vector, $\boldsymbol{E}$, and the magnetic field vector, $\boldsymbol{H}$. Transmitting electric current antennas can be modelled as electric current sources, while transmitting electric current loop antennas can often be modelled as magnetic current sources with a magnetic moment that depends on the electric current strength. For this reason, the source volume densities of the electric current, $\boldsymbol{J}^e$, and magnetic current, $\boldsymbol{J}^m$, are introduced in Maxwell's equations as

$$-\nabla \times \boldsymbol{H} + (\sigma + \varepsilon \partial_t)\,\boldsymbol{E} = -\boldsymbol{J}^e, \tag{2-1}$$

$$\nabla \times \boldsymbol{E} + \mu \partial_t \boldsymbol{H} = -\boldsymbol{J}^m, \tag{2-2}$$

where the medium parameters are the electrical conductivity σ in S/m, the electric permittivity ϵ in F/m and the magnetic permeability μ in H/m. Using these equations, we assume that the earth responds instantaneously to the electromagnetic disturbance. [26]

In this thesis we work with an instrument in mind that has a single frequency of operation. We therefore transform the Maxwell equations to the frequency domain, using an $\exp(i\omega t)$ time dependence. The resulting equations are given by

$$-\nabla \times \hat{\boldsymbol{H}} + (\sigma + i\omega\varepsilon)\hat{\boldsymbol{E}} = -\hat{\boldsymbol{J}}^e, \tag{2-3}$$

$$\nabla \times \hat{\boldsymbol{E}} + i\omega\mu\hat{\boldsymbol{H}} = -\hat{\boldsymbol{J}}^m. \tag{2-4}$$

We work with frequencies such that $\sigma \gg \omega\varepsilon$ such that we can neglect the $i\omega\varepsilon$-term in equation (2-3). This is known as the diffusive field approximation as explained below.

2-2   Influence of physical properties

According to the Maxwell's equations, three macroscopic physical properties need to be considered to describe the behaviour of the electromagnetic (EM) field. These are the electrical conductivity, σ, the electric permittivity, ϵ, and the magnetic permeability, μ. Although the conductivity can be treated as constant over large range of frequencies, the two other physical properties show a significant variation with frequency and complex behaviour.

As stated above, we work with the diffusive field approximation, where the electric permittivity vanishes ($\epsilon = 0$). For most natural soils, electrical conductivity varies from 1 S/m in tidal areas to 10^{-4} S/m for crystalline rocks[14] or permafrost. In the current state, considering the frequency range of 3 kHz - 300 kHz and soil bulk conductivity values of $10^{-4} < \sigma < 1$, we can use the diffusive field approximation.

The magnetic permeability is assumed to be equal to its free-space value. This is a proper assumption for most natural earth materials and only for certain types of metals can this value deviate considerably from its free-space value. Hence we assume that $\mu = \mu_0$.

2-3   Computation of the layered earth response

Most near surface frequency domain electromagnetic instruments allow an interpretation that is limited to a small lateral vicinity and some depth range. For such a limited range, a horizontally layered earth model can be an adequate model. This is the model for which we give here the general mathematical formulation for the vertical magnetic field generated by a vertical magnetic dipole.

The analytical method that allows calculations of the electromagnetic field at the surface of a homogeneous earth for either a magnetic dipole source or an electric dipole source has been known for years[27]. Without loss of generality, the vertical magnetic field component in the subsurface reflection response generated by a vertical magnetic dipole is given by

$$H_z^s(r,h,\omega) = \frac{M_z}{4\pi} \int_0^\infty \lambda^2 R_0(\lambda) e^{-\lambda h} J_0(\lambda r) d\lambda, \tag{2-5}$$

where R_0 is the subsurface reflection response at the ground surface, J_0 is the Bessel function of the first kind and order zero, r is the distance between source and receiver points in the horizontal plane and h is the vertical distance from source to receiver via the surface. The general reflection response is given by the recursive formula as

$$R_n(\lambda) = \frac{r_n + R_{n+1} \exp(-2\gamma_{n+1} d_{n+1})}{1 + r_n R_{n+1} \exp(-2\gamma_{n+1} d_{n+1})}, \tag{2-6}$$

where r_n is the local reflection coefficient at depth level z_n, the layer thickness, d_n, is given by $d_n = z_n - z_{n-1}$ and the vertical wavenumber is given by $\gamma_n = \sqrt{i\omega\sigma_n\mu_0}$. The surface reflection response, R_0, is recursively computed by starting at the bottom boundary where, N, by $R_N = r_N$. The local reflection coefficient at z_n is given by

$$r_n = \frac{\gamma_n - \gamma_{n+1}}{\gamma_n + \gamma_{n+1}}, \tag{2-7}$$

The Hankel transform is calculated numerically by the digital linear filter method[15] [9] [29].

2-3-1 Low Induction Number (LIN) Approximation

This approximation lies at the basis of the work undertaking by Bellugi (1949) and Wait (1951), which had a big role in the interpretation of EM-frequency-domain exploration techniques in mining geophysics [7]. When considering a homogeneous half space and both antennas place on the ground surface, it is possible to evaluate the integral analytically to obtain very simple expressions that illustrate the roles of frequency and conductivity. For example, in the horizontal co-planar (HCP) configuration, the response is expressed as the ratio of the vertical secondary field H_z^s to the primary field H_z^p:

$$\frac{H_z^s}{H_z^p} = r^3 \int_0^\infty \lambda^2 \frac{\lambda - \gamma_1}{\lambda + \gamma_1} J_0(\lambda r) d.\lambda \tag{2-8}$$

Eq. (2-8) is evaluated as

$$\frac{H_z^s}{H_z^p} = \frac{2}{(\gamma_1 r)^2} [9 - (9 + 9\gamma_1 r + 4(\gamma_1 r)^2 + (\gamma_1 r)^3) \exp(-\gamma_1 r)] - 1. \tag{2-9}$$

The LIN approximation is obtained by performing a Taylor series expansion on this expression around $\gamma_1 r = 0$ and we obtain

$$\frac{H_z^s}{H_z^p} \cong -\frac{\gamma^2 r^2}{4} + \frac{4\gamma^3 r^3}{15}. \tag{2-10}$$

With the LIN assumption, where $\gamma_1 r << 1$, Eq. (2-10) established that the response is in quadrature and proportional to the conductivity, the frequency and the square of the coil separation, see Eq. (2-11).

$$\frac{H_{xs}}{|H_{zp}|} \cong -\frac{\gamma^2 r^2}{4} = -\frac{i\sigma\mu_0\omega r^2}{4} \tag{2-11}$$

Eq. (2-10) also clarifies that if one or multiple of these parameters are increasing, then the part of the highest term, which is the real part here, increases. This results in the loss of linearity and in the rotation of phase of the response. Eq. (2-10) is a very useful equation for understanding the physical meaning of the measurements as long as the LIN approximation is valid.

Chapter 3

Methodology and Validation

Apparent conductivity forward modelling is usually performed under the low induction number condition ($<$ 100 mS/m) using the McNeill (1980) model, which is based on some simplified assumptions. With the high induction number condition (> 100 mS/m)[10], a more complex model is allowed. In this study we use the full-EM model, which is valid for both low and high induction number conditions[16].

3-1 Multi-receiver EM induction sensor

A measure of apparent conductivity distribution in the subsurface space is called cumulative response[18]. With regard to this, sensitivity curves have been introduced by McNeill (1980), which are used to model the cumulative response of the electromagnetic field generated by EM instruments considering the HCP and VCP modes. In a low induction condition, the effective penetration depths in HCP and VCP modes are calculated considering inter coil spacing[3].
A multi-configuration EM sensor called CMD-Explorer (GF Instruments) was considered to simulate the HCP EM response for two synthethic data sets. This system results in EM responses for three different offsets. It's operating frequency is 10 kHz and the coil centers were assumed to be 21 cm above the ground.

3-2 Inversion procedure

Since the CMD-Explorer has three receiving antennas, we cannot expect more information than of an estimate three-layered model where the first and second layer are defined , and the final layer is set to infinity (see Figure 3-1. This results in five medium parameters, $\sigma_1, \sigma_2, \sigma_3, d_1$ and d_2, which can be used to calculate the EM response from Eq. (2-5) using the global reflection coefficient in Eq. (2-6) and the so-called Fast Hankel Transform filter table. Considering five medium parameters, Eq. (2-5) has been used to create a 5-dimensional solution space of all possible combinations of conductivity values and thicknesses within a predefined range. For the conductivity we generate three logarithmically spaced vectors ranging from 10^{-3} S/m to 10-0.5 S/m with 91 number of data points. The thicknesses are stored in two linearly spaced vectors ranging from 0.0 m to 5.0 m with 51 number of data points. Then for all the possible combinations of conductivity's and thicknesses the three EM responses have been calculated and stored in a database.
When data has been recorded from the instrument, it can produce three complex values after back-calculation. The measured apparent conductivity is being used to calculate the complex values using Eq. (2-10) and Eq. (2-11).

Finally, we use the created database to find which combination of five medium parameters has the three complex values that matches the measurements the best in the least square sense.

In this report we distinguish two different inversion methods:

1. **Constrained database approach**: for this we define a thickness range in which we will constrain the thicknesses of the neighbouring data points after going through the full database for the first data point. Depending on the predefined thickness range, the inversion will search the best fit of the 5-dimensional space in the constrained data base. This method is proposed with the assumption that there are no abrupt changes in the continuity of layers.

2. **Full database approach**: for this method the full database is being used to determine the best fit. Since this method is more comprehensive it takes more time than the constrained database approach.

In order to investigate the behaviour of the two inversion algorithms, two sets of synthetic data were generated and subsequently inverted and compared. These models are mainly based on geological settings that could occur in the field.
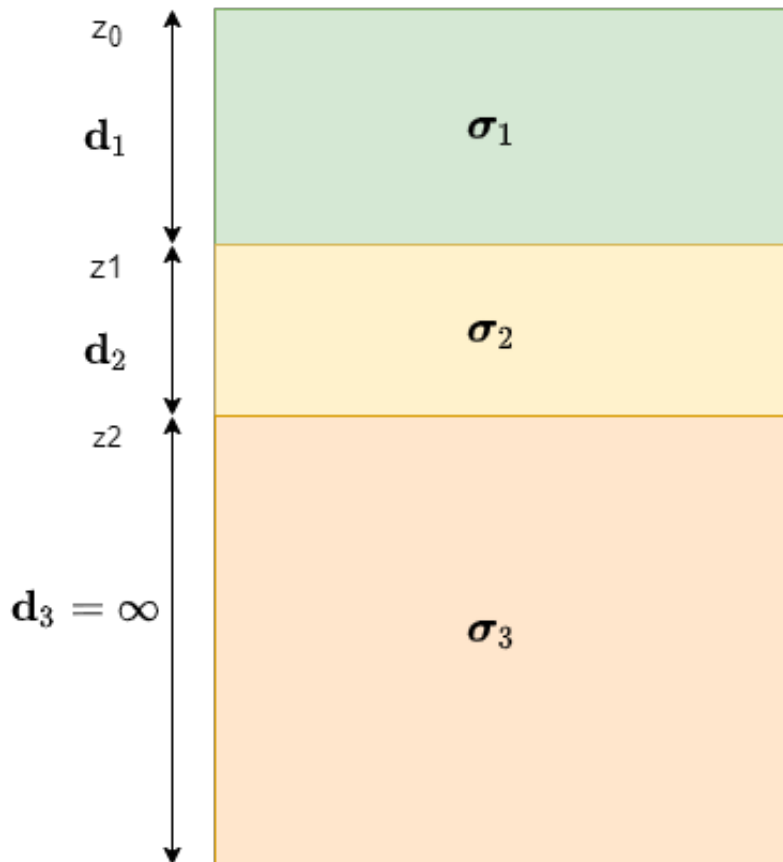
Figure 3-1: Schematic view of a three layered earth model.

3-3   Synthetic data set test

For the inversion of these synthetic data sets both the constrained database and the full database methods have been applied. The thickness range of the constrained method has been set to 1.4 m, this means for every obtained model for a data point, the solution for the next data point is being searched in +/- 0.7 m of the found thicknesses.

Synthetic model 1
The first model contains a conductive layer on top of a less conductive layer with a resistive lens interrupting the layers. The first, second and third layer have conductivity values of 0.05, 0.005 and 0.02 S/m, and the resistive lens has a conductivity of 0.0009 S/m. Their corresponding layer thicknesses are varying from 1-2 m for the first layer, 2-3 m for the second layer and the third layer is set to infinity.

Data obtained from the forward modelling is presented in Figure 3-2. Five model parameters, three layer conductivity's and two thicknesses were used. Sensitivity analysis can show us whether all model parameters are resolved. Here, the root-mean-square error (RMSE) is used to analyze the different methods.

The results of both inversion methods clearly demonstrate some of the advantages and disadvantages of the different inversion methods.

The full database inversion provides us a good estimate of the thicknesses of the first and second layer (see Figure 3-3b) relative to the constrained database inversion, which overestimates the thickness of the second layer (see Figure 3-3a). Also the resistive lens is accurately reconstructed on location with the full database inversion.

The constrained inversions shows a RMSE of 0.335 for the first layer and 1.526 for the second layer. Whereas the full database inversion shows 0.333 and 0.359, respectively for the first and second layer. The data misfit for both methods of the EM responses is shown in Figure 5-1a.

The computation time for the full database method was 19.65 minutes whereas the constrained method can be accomplished in 7.8 minutes.
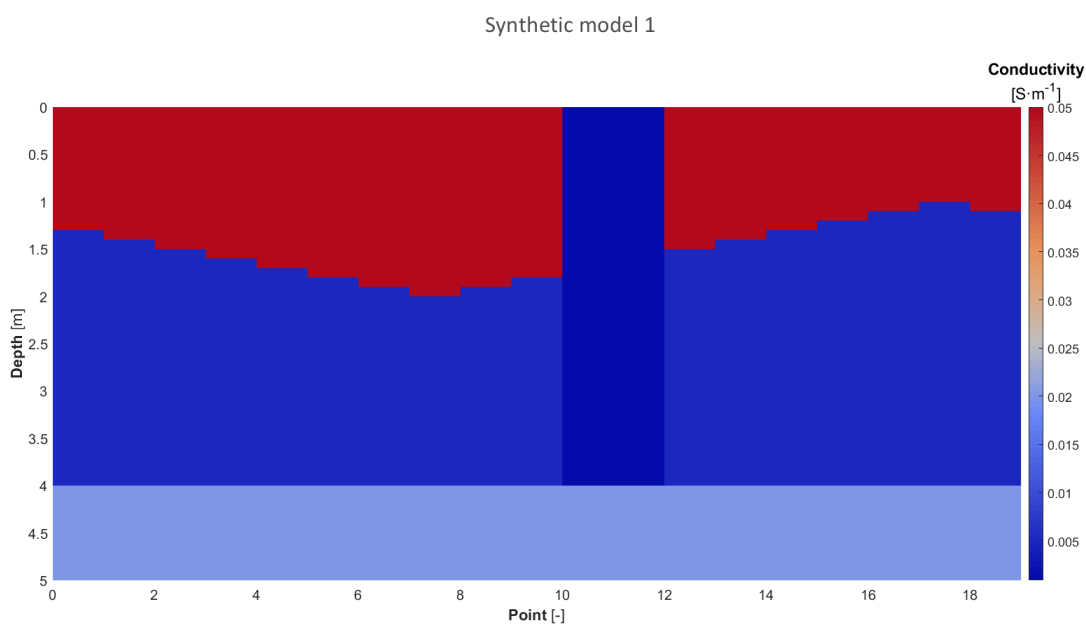
Figure 3-2: Synthetic model 1.

Model 1 (constrained method)

(a)

Model 1 (full database method)
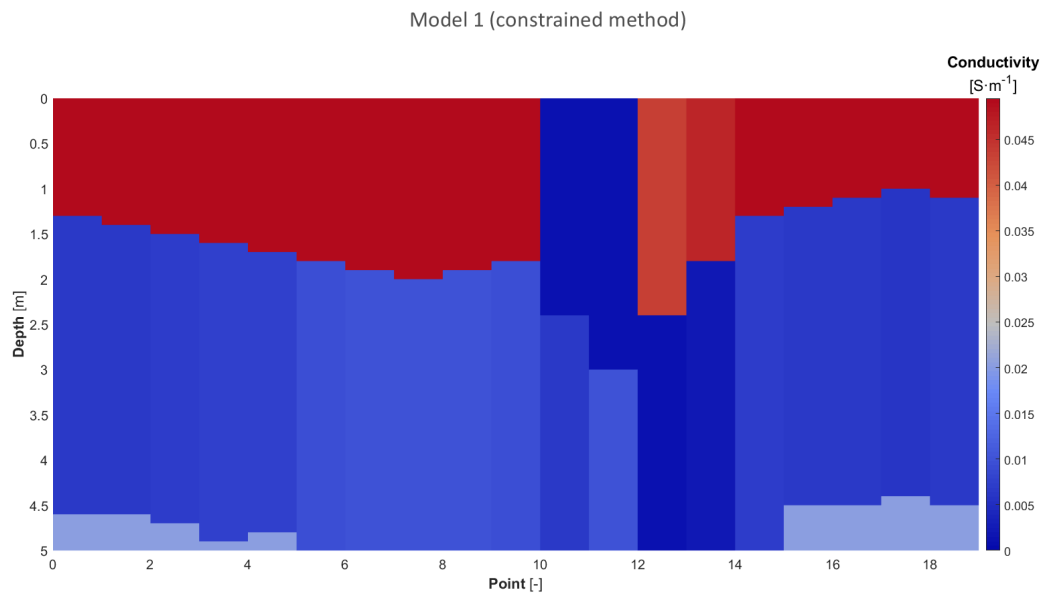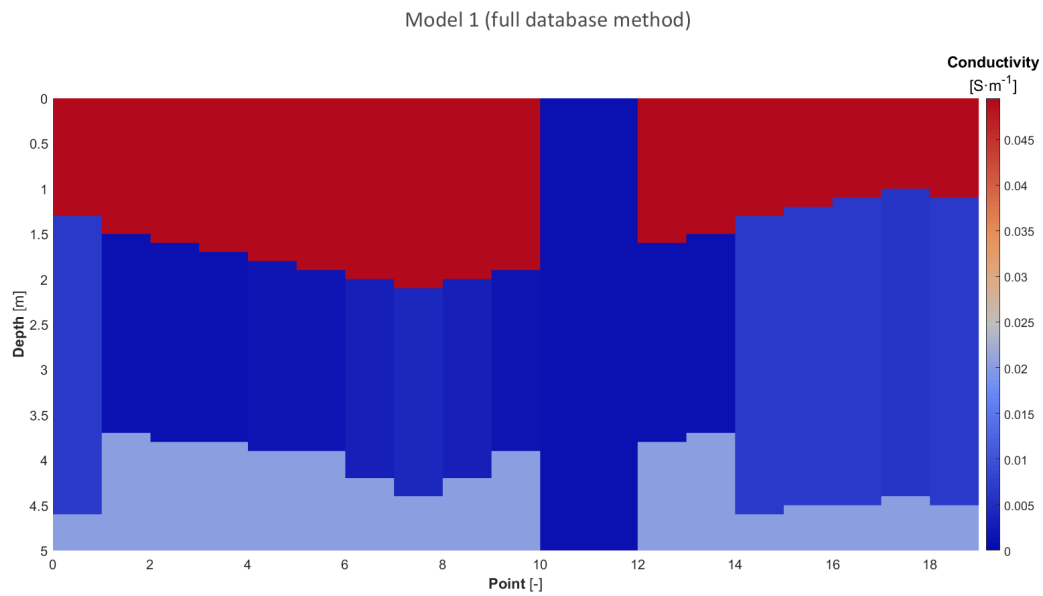
(b)

Figure 3-3: (a) Constrained inverted conductivity model 1 (b) Full database inverted conductivity model 1

Synthetic model 2

The second synthetic model consists of a section where the same conductive layer, as described for synthetic model 1, is on top of a less conductive layer, a less conductive layer on top of a conductive layer and a conductive lens (see Figure) 3-4. It has the same conductivity values as defined for the first synthetic model except for the conductive lens, which has a conductivity of 0.2 S/m. It's corresponding layer thicknesses are varying in between 0.3 to 3 m for the first layer, 0 to 2.1 m for the second layer and the final layer is set to infinity.

Data obtained from forward modelling is presented in Figure 3-4. Comparing Figures 3-5a and 3-5b we can see that our top layer is well estimated for both approaches, however the second layer is locally overestimated by the constrained method. Surprisingly, the thickness of the conductive lens is well estimated for both methods. The constrained inversions shows a RMSE (root-mean-square error) of 0.482 for the first layer and 1.709 for the second layer. Whereas the full database inversion shows 0.558 and 1.066, respectively for the first and second layer. The computation time for the full database method was 24.56 minutes for the first this model whereas the constrained method can be accomplished in 8.8 minutes.
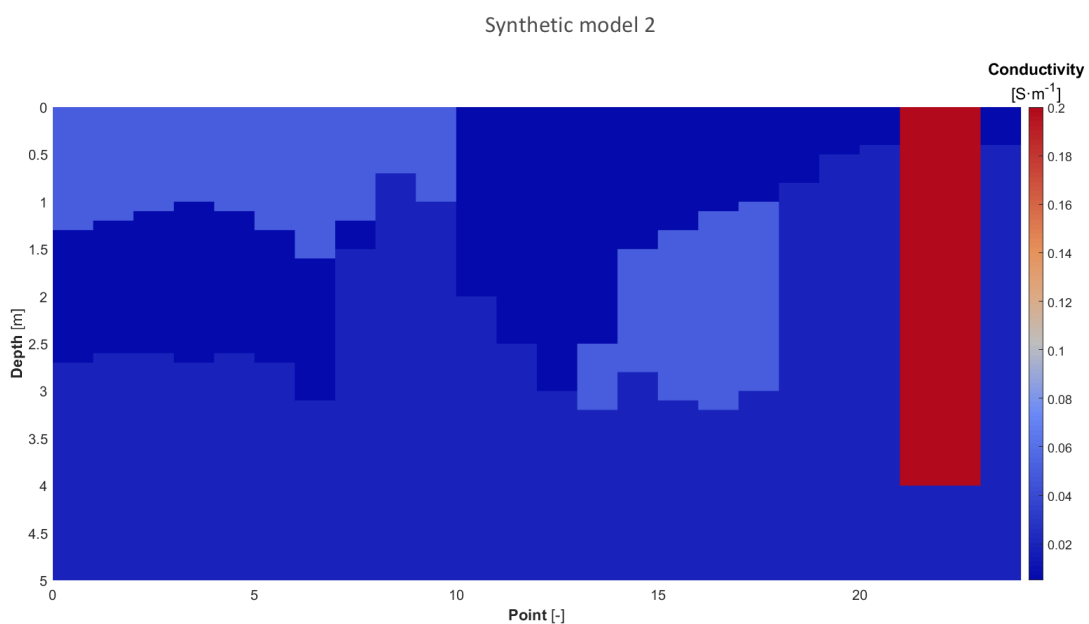
Figure 3-4: Synthetic model 2.
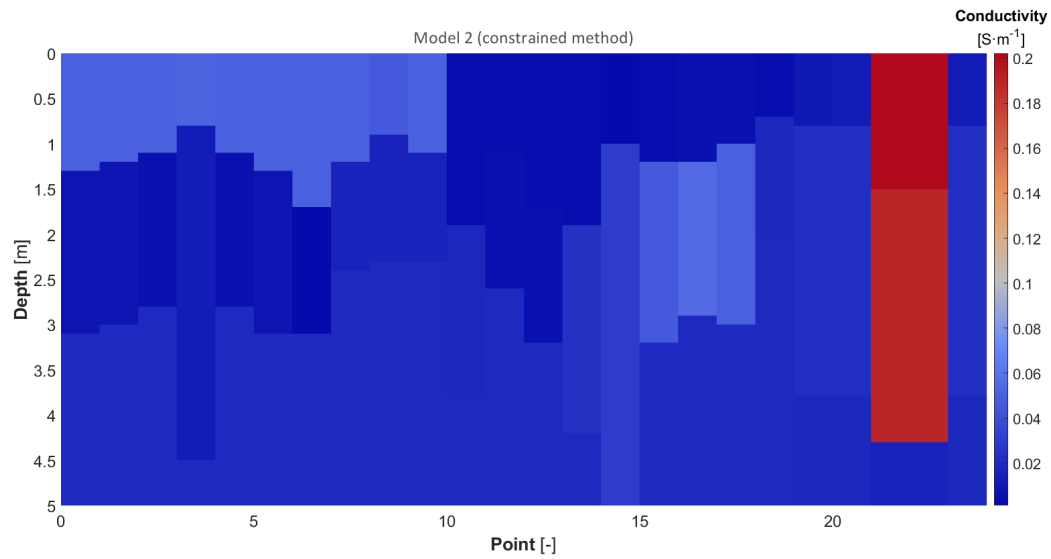
(a) -
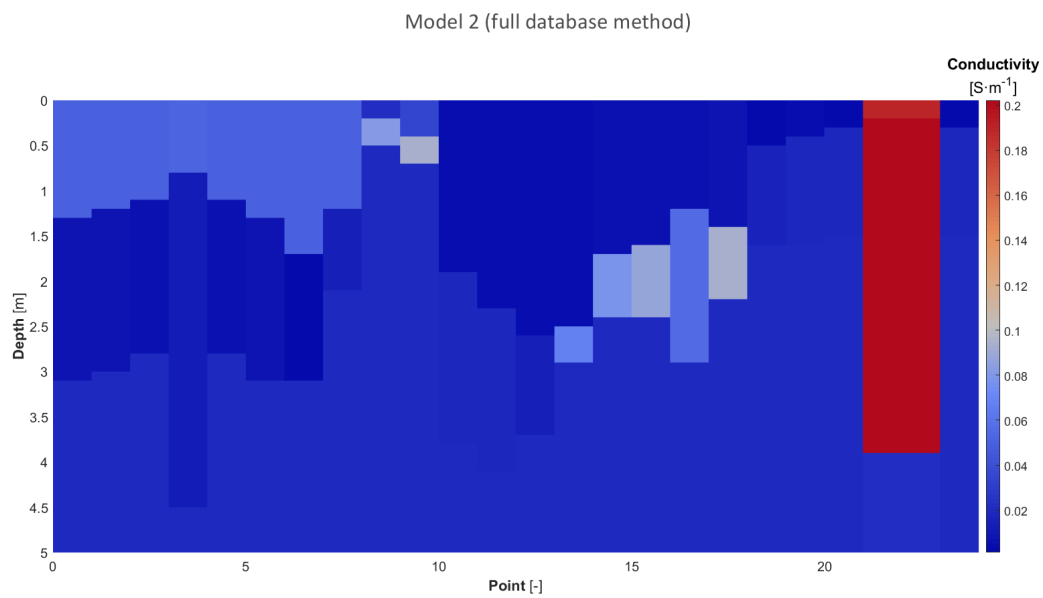
(b)

Figure 3-5: (a) Constrained inverted conductivity model 2 2 (b) Full database inverted conductivity model 2

Chapter 4

Results

4-1 Field study 1

4-1-1 Inversion of field data

Two FDEM and ERT field line data sets, each with a length of 110 m, were collected in the eastern part of the Netherlands. The measurements were collected from east to west directed towards a channel. The area's apparent conductivity values are varying in between 1.05 mS/m to 18.7 mS/m. For ERT, we used the dipole-dipole configuration, which has in general a good vertical resolution and enabled us to take a larger number of measurements using the multi-channel capability of ABEM Terrameter LS2. The roll-along technique was used to combine measurements. The roll-along measurements were configured so that no electrode was measured twice. The measurements from the roll-along survey were combined into one data set.

Along the ERT transect, EM induction measurements were conducted, on ground, every second with the CMD-MiniExplorer in HCP configuration. The CMD-MiniExplorer operates at a frequency of 30 kHz and has three receiver antennas, with separations of 0.32, 0.71 and 1.18 m. The HCP configuration was calibrated by keeping the system in the air and on the ground according to the specifications made by the manufacturer (GF Instruments).

For this FDEM measurements we simultaneously geo-referenced the data points using a the Leica iCON GPS 70 series.

4-1-2 Comparison of FDEM vs ERT measurements

Inaccurate readings due to poorly coupled electrodes or current injection problems during ERT measurements were removed. This data set was inverted using the robust inversion method of the RES2DINV software[17] with default damping parameters. The robust inversion scheme that uses the L-1 norm for data and model space was used taking into account sharp layering boundaries. The inverted profiles shown in Figures 4-1b and 4-2b have a mean square error of 2.62 and 2.85 % respectively.

The ERT profiles in Figures 4-1b and 4-2b shows in general a spatial of decrease of electrical resistivity. These electrical resistivity changes can be related to changing soil water content and changes in texture. Furthermore, the electrical resistivity decreases with depth, which corresponds to an increase in water and/or clay content with depth. The upper (red) layer has electrical resistivity values of 2000-5000+ $\Omega \cdot m$, the lower (green) layer has values of 150-800 $\Omega \cdot m$

and the bottom layer (blue has values of 10-150 $\Omega \cdot m$.

It is remarkable that the more we approach the channel (west), the more the electrical resistivity values are decreasing. This is possibly because of water intrusion from the channel.

Figures 4-1a and 4-2a show modelled electrical resistivity profiles obtained through the full data base inversion. These modelled electrical resistivity values are consistent with the ERT profiles shown in Figure 4-1b and 4-2b, however limited by depth. This is due to the high frequency (30 kHz) of this instrument and the smaller separations of the receiver antennas compared to the CMD-Explorer.

(a) -

(b)
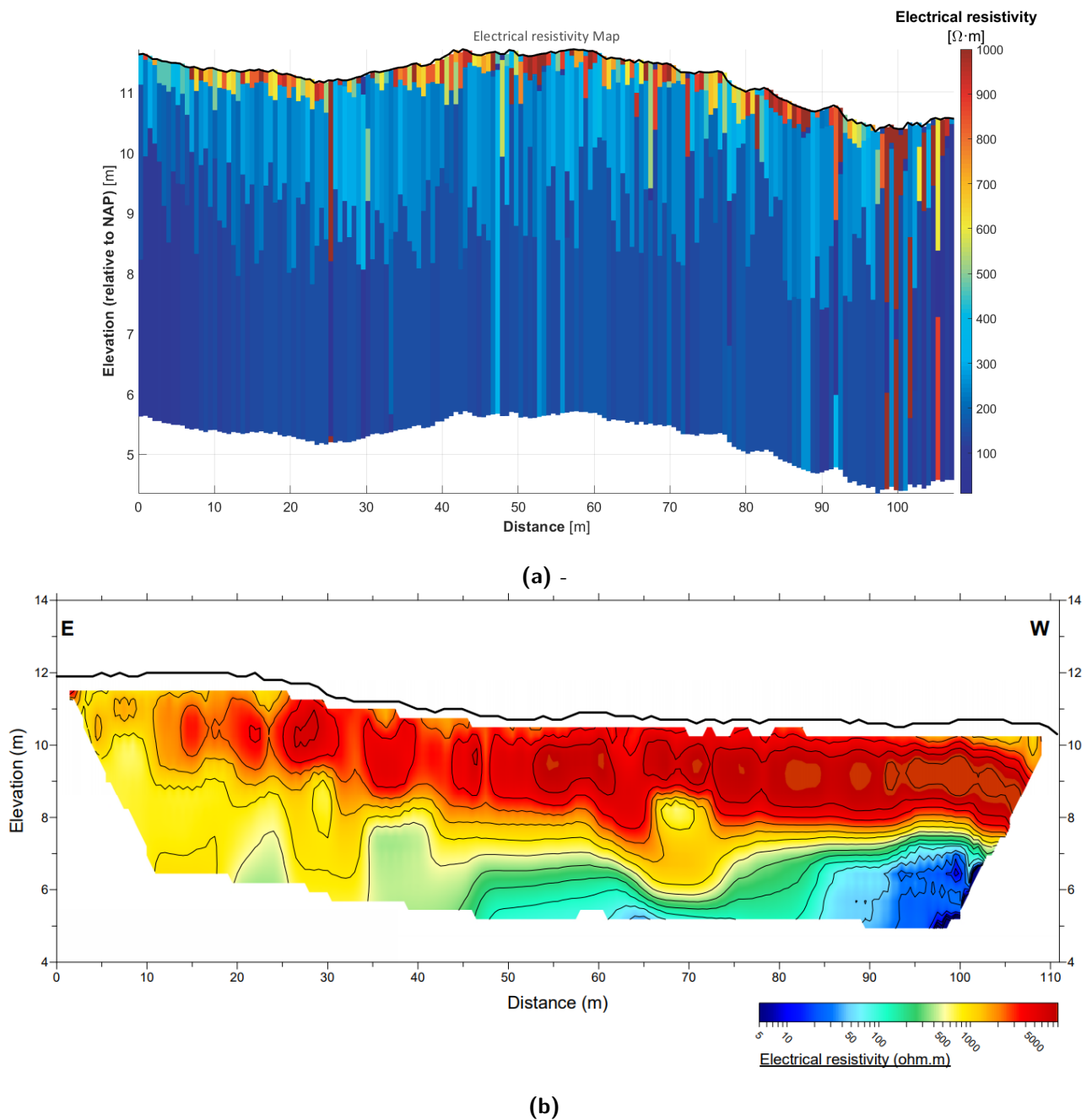
Figure 4-1: (a) Full database inverted resistivity mode line 1(b) ERT measurement line 1

(a) -

(b)
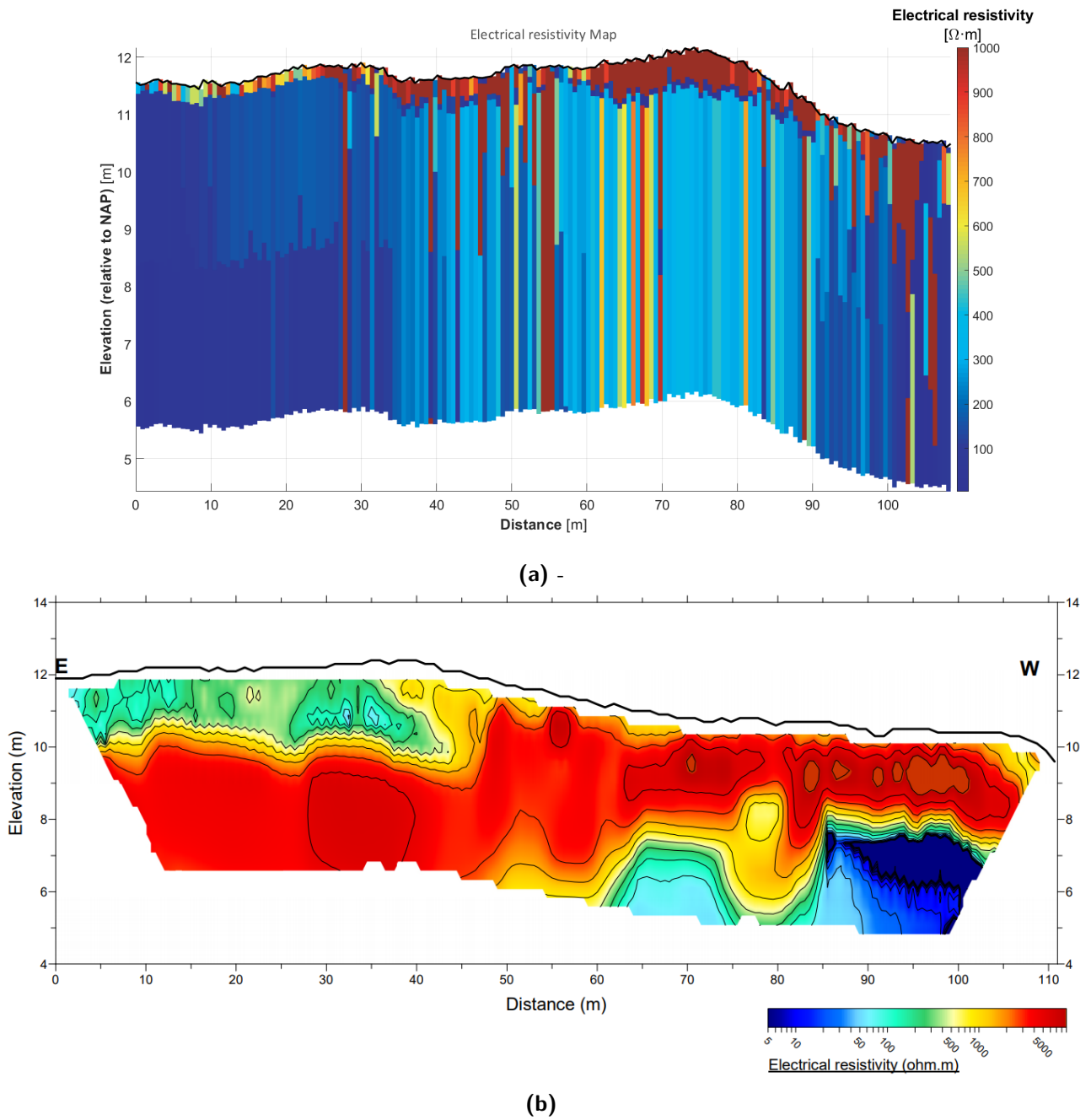
Figure 4-2: (a) Full database inverted resistivity mode line 2 (b) ERT measurement line 2

4-2 Field Study 2

This field study is executed in an area located in the northern part of the Netherlands. The area can be compared to the polder situation stated in Figure 1-1 and so we can expect the existence of an clayey top layer. The CMD-Explorer has been used to perform the measurements at a height of 21 cm from the ground in HCP configuration. Apparent conductivity measurements shows variations from -18.2 mS/m to 16.78 mS/m. The comparison of measurements with a different depth of investigation can provide information about the soil build-up, or about the in- or decrease of conductive sediments with depth. The CMD-Explorer operates at a frequency of 10 kHZ and has three receiver antennas, with separations of 1.48, 2.82 and 4.49 m. For this FDEM measurements we simultaneously, every second, geo-referenced the data points using a the Leica iCON GPS 70 series.

Five hand drills, which classified in field, were performed until 5 meter of depth. These hand drilling data set is integrated in the inverted full database conductivity model obtained for this EM measurements for comparison (see Figure 4-3) . The hand drill data sets are compared to the inverted full database method for verification.

4-2-1 Comparison of inverted field data with hand drills for verification

From Figure 4-3 we can see that the inverted model has a continuous high conductive layer at the bottom. Above this layer we find a low conductive layer, sometimes interrupted by lenses. On top again a high conductive layer is part of the profile. Those lenses might indicate magnetic activity in soils (pollution).

The conductive bottom layer might indicate saturated soil. The groundwater level is known, from hand drill data, to vary in between -0.40 m to -0.60 m.

The hand drilling showed a thin humous top layer varying from 0.2 to 0.8 meter for some of the hand drills. Also the top layers, despite being classified as sand (yellow) as main constituent, contain a significant amount of clay. However when the last clay (green) layer was reached, only sand was found, which was moderately silty. Furthermore, the interface present with the borehole data do not agree with the all the interfaces found with the inversion. This might be due to the highly conductive top layer (humous layer), which will reduce the depth of penetration. Also one should take into account that the hand drill data is more detailed compared to the model.
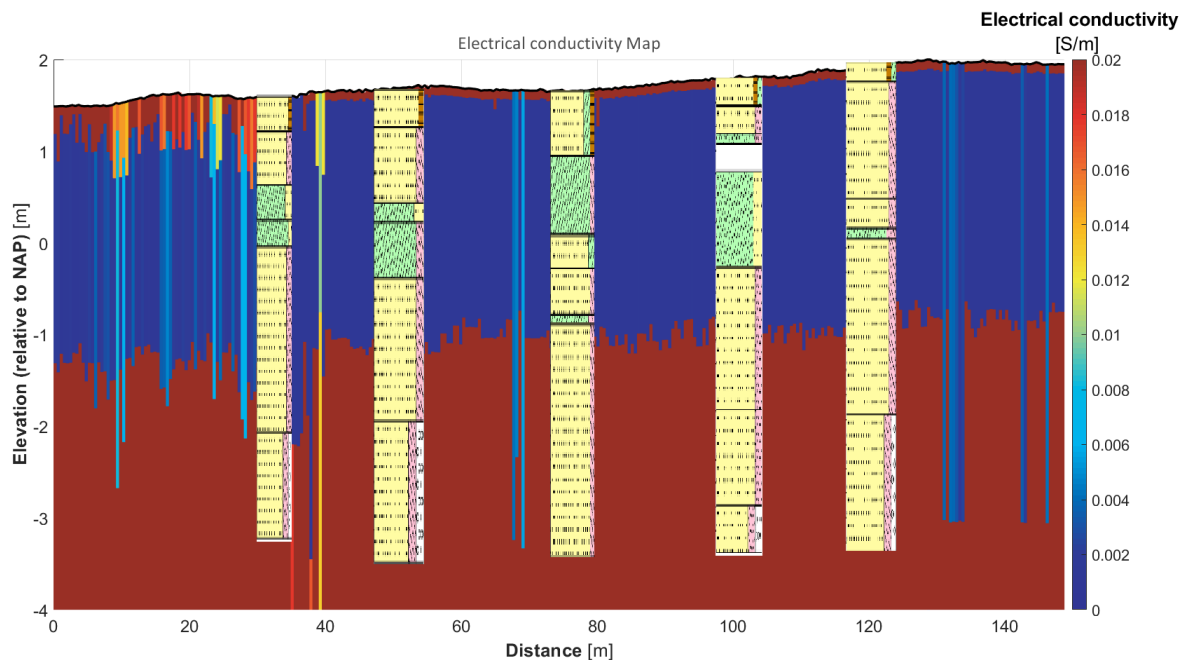
Figure 4-3: Inversion result from the measured transect integrated with hand drill data.

Chapter 5

Discussion and conclusions

Synthetic data set Two synthetic data sets were generated to mimic conductive and resistive top layers. The ability to reconstruct these layers for both the inversion approaches have been studied. Figure 5-1 shows us the difference in the data misfit for both the approached inversion methods. It can be seen that in general the methods were able to recover the synthetic model well. However the constrained data base inversion shows difficulties when approaching a resistive lens. This can be seen in Figure 5-1a where the data misfit increases. In order to improve the constrained method inversion, one could try to find the optimum thickness range by using for example the Pythagorean theory to estimate a possible thickness range by using the distance between every two neighbouring data points.

The full database inversion showed us promising results, however compared to the constrained method this method is time-consuming. To improve the match to a 1D model, common-midpoint (CMP) sorting could be done if spacing between measurements are small enough. This can be done for acquisition with the instrument on the ground and with the instrument at some elevation above the ground. The measurement is quite sensitive to the distance of the instrument above the ground and this should be carefully measured and more databases will be required.

(a)

(b)
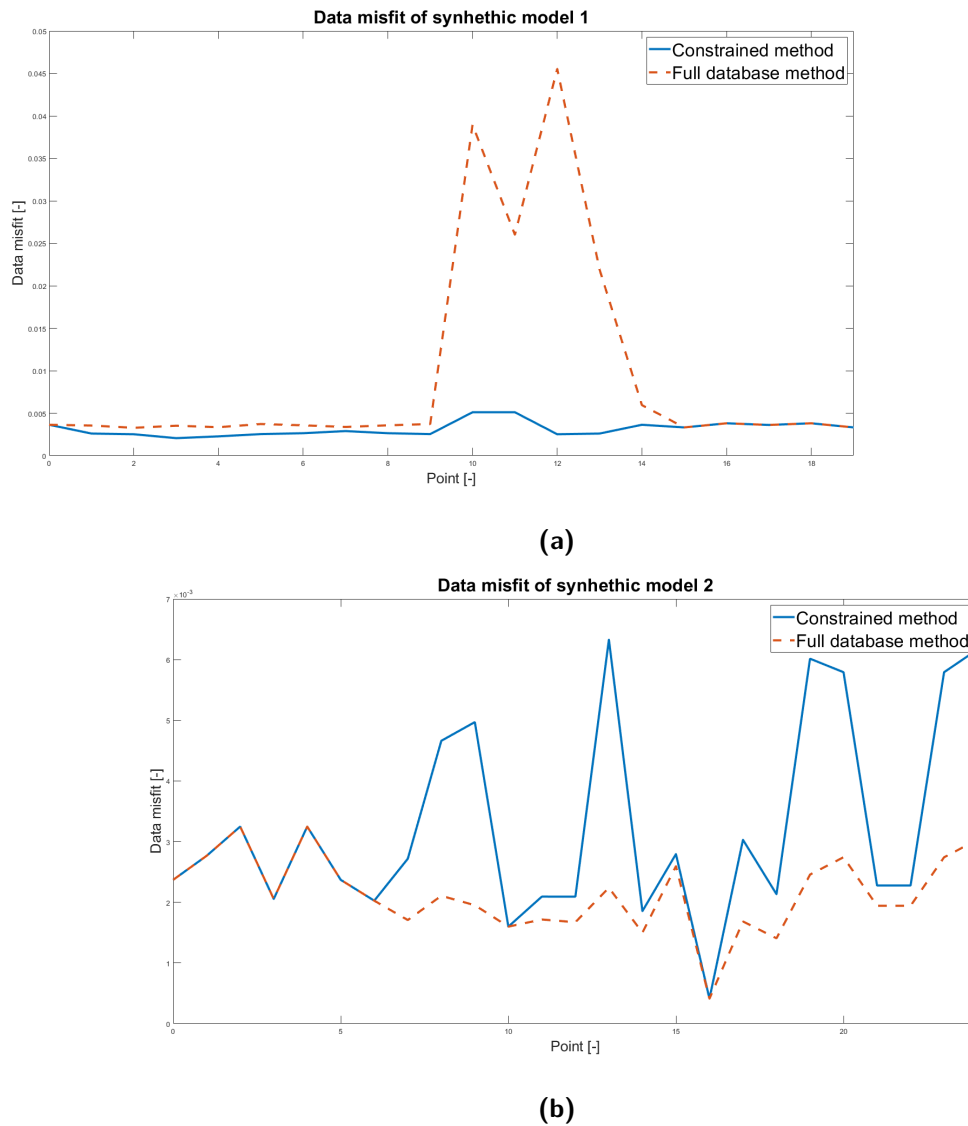
Figure 5-1: (a) Data misfit plot for synthetic model 1 (b) Data misfit plot for synthetic model 2

ERT vs EM

ERT and EM induction measurements were carried out on a test site with low lateral and higher vertical variation in electrical conductivity. A comparison of the measured EM induction apparent conductivity's with modelled electrical resistivty's showed that the trends are very similar and the full database inversion method did recover two layers, and there corresponding thicknesses.

However, a clear shift was present for the measured EM induction data, such that the EM induction values cannot be quantitatively interpreted directly. Reliable quantitative values are vital for making a layered inversion using HCP measurements, and so top layer estimation possible. Any static shift will have a significant influence on the inversion results. Having quantitative EM induction values and the possibility of acquiring EM induction data on large-scales offers great potential for a wide range of applications. Nevertheless, more measurements at different sites must be performed to investigate the reliability of the inversion approaches proposed here. Also measuring in different configurations can be done to increase ability of reconstructing layers accurate through inversion.

EM vs Hand drill data EM and hand drilling were carried out on a test site next to a dike in the Netherlands. The aim of this study was to reconstruct the (top) clay layer. Hand drill data were used as verification for this. Except for the first measuring points, we were not able to recover the top layer from a distance of approximately 40 m (see Figure 4-3). From hand drill data we know that on average the ground water level was -0.40 m to -0.60 m relative to NAP, which is approximately 2 m from the surface for the area. Depending on whether the water is contaminated or not this can have a huge impact on the inversion, which in this case resulted in electrical conductivity values of 0.02 S/m for both the top and bottom layer. In order to be able to correct the model for groundwater, one can measure the electrical conductivity of groundwater on site and subsequently using it as correction for your model. Depending on it's properties, also the humous top layer could have a significant impact on the EM data.

Bibliography

[1] William Bleam. Clay mineralogy and chemistry. In *Soil and Environmental Chemistry*, pages 87–146. Elsevier, 2017.

[2] D.J. Brus, M. Knotters, W.A. van Dooremolen, P. van Kernebeek, and R.J.M. van Seeters. The use of electromagnetic measurements of apparent soil electrical conductivity to predict the boulder clay depth. *Geoderma*, 55(1-2):79–93, October 1992.

[3] James Callegary, Ty Ferré, and Ross Groom. Vertical spatial sensitivity and exploration depth of low-induction-number electromagnetic-induction instruments. *Vadose Zone Journal*, 6:158–167, 02 2007.

[4] John Connolly and Nicholas Holden. Object oriented classification of disturbance on raised bogs in the irish midlands using medium- and high-resolution satellite imagery. *Irish Geography*, 44:111–135, 03 2011.

[5] James A. Doolittle and Eric C. Brevik. The use of electromagnetic induction techniques in soils studies. *Geoderma*, 223-225:33–45, July 2014.

[6] Technical Advisory Committee for Flood Defense in the Netherlands. Clay for dikes. Technical report, The Road and Hydraulic Engineering Institute, 05 1996.

[7] Frank C. Frischknecht, Victor F. Labson, Brian R. Spies, and Walter L. Anderson. 3. profiling methods using small sources. In *Electromagnetic Methods in Applied Geophysics*, pages 105–270. Society of Exploration Geophysicists, January 1991.

[8] Jan L. Gunnink and Bernhard Siemon. Applying airborne electromagnetics in 3d stochastic geohydrological modelling for determining groundwater protection. *Near Surface Geophysics*, 13(1):45–60, August 2014.

[9] D. Guptasarma and B. Singh. New digital linear filters for hankel j 0 and j 1 transforms. *Geophysical Prospecting*, 45(5):745–762, September 1997.

[10] Jan Hendrickx, Brian Borchers, Dennis Corwin, Scott Lesch, A.C. Hilgendorf, and J. Schlue. Inversion of soil conductivity profiles from electromagnetic induction measurements. *Soil Sci. Soc. Am. J.*, 66, 01 2002.

[11] John Householder, John Janovec, Mathias Tobler, Susan Page, and Outi Lähteenoja. Peatlands of the madre de dios river of peru: Distribution, geomorphology, and habitat diversity. *Wetlands*, 32:359–368, 04 2012.

[12] M. HOWELL. *A SOIL CONDUCTIVITY METER*, volume 9. Wiley, June 1966.

[13] A Keaney, Jennifer Mckinley, Conor Graham, M. Robinson, and Alastair Ruffell. Spatial statistics to estimate peat thickness using airborne radiometric data. *Spatial Statistics*, pages –, 08 2013.

[14] Keller. *Electromagnetic Methods in Applied Geophysics*. Society of Exploration Geophysicists, January 1988.

[15] O. KOEFOED. A NOTE ON THE LINEAR FILTER METHOD OF INTERPRETING RESISTIVITY SOUNDING DATA*.GeophysicalProspecting*, 20(2) : 403 − −405, June1972.

[16] Jan Kruk, J.A.C. Meekes, P.M. Berg, and J.T. Fokkema. An apparent‐resistivity concept for low‐frequency electromagnetic sounding techniques. *Geophysical Prospecting*, 48:1033 – 1052, 11 2000.

[17] Meng Loke, Richard Acworth, and Torleif Dahlin. A comparison of smooth and blocky inversion methods in 2d electrical imaging surveys. *Exploration Geophysics*, 34:182–187, 01 2003.

[18] J McNeill. Electromagnetic terrain conductivity measurement at low induction numbers. *Geonics Limited, Technical Note TN-6, Mississauga*, 6, 01 1980.

[19] James K. Mitchell and Kenichi Soga. *Fundamentals of Soil Behavior*. 05 2005.

[20] C. Parchas and Alain Tabbagh. Simultaneous measurements of electrical conductivity and magnetic susceptibility of the ground in electromagnetic prospecting. *Archaeo-Physika*, 10:682–691, 01 1978.

[21] L. E. Parry, L. J. West, J. Holden, and P. J. Chapman. Evaluating approaches for estimating peat depth. *Journal of Geophysical Research: Biogeosciences*, 119(4):567–576, April 2014.

[22] Andrew Parsekian, Lee Slater, and Daniel Giménez. Application of ground-penetrating radar to measure near-saturation soil water content in peat soils. *Water Resources Research*, 48:2533–, 02 2012.

[23] William Powrie. *Soil Mechanics*. 08 2004.

[24] J. D. Rhoades and D. L. Corwin. Determining soil electrical conductivity-depth relations using an inductive electromagnetic soil conductivity meter. *Soil Science Society of America Journal*, 45(2):255–260, March 1981.

[25] Keith Sheets and Jan Hendrickx. Noninvasive soil water content measurement using electromagnetic induction. *Water Resources Research*, 31:2401–2409, 10 1995.

[26] Evert Slob. Electromagnetic Exploration Metods, Lecture Notes, 2018.

[27] A. Sommerfeld. Über die ausbreitung der wellen in der drahtlosen telegraphie. *Annalen der Physik*, 386(25):1135–1153, 1926.

[28] M. S. TITE and C. MULLINS. ELECTROMAGNETIC PROSPECTING ON ARCHAEOLOGICAL SITES USING a SOIL CONDUCTIVITY METER. *Archaeometry*, 12(1):97–104, February 1970.

[29] Dieter Werthmüller, Kerry Key, and Evert C. Slob. A tool for designing digital filters for the hankel and fourier transforms in potential, diffusive, and wavefield modeling. *GEOPHYSICS*, 84(2):F47–F56, March 2019.

[30] BG Williams and D Hoey. The use of electromagnetic induction to detect the spatial variability of the salt and clay contents of soils. *Soil Research*, 25(1):21, 1987.